# Mechanistic Aspects of GFP Chromophore Biogenesis

Rebekka M. Wachter*
Department of Chemistry and Biochemistry, Arizona State University, Tempe, AZ, USA 85287

## ABSTRACT

We have investigated the autocatalytic mechanism of green fluorescent protein (GFP) maturation. To this end, we have used techniques such as site-directed mutagenesis, X-ray crystallography and in vitro kinetics, and have monitored the reaction by fluorescence, HPLC and MALDI (matrix-assisted laser desorption ionization) mass spectrometry. In summary, we find that chromophore formation, which generally occurs within 40 to 60 min, can be accelerated dramatically under some conditions. In the E222Q variant, the rate-limiting process appears to be a function of slow proton transfer steps. Other mutagenesis data indicate that chromophore biogenesis is not driven by the aromatic character of residue 66. The GFP self-modification process involves a rate-limiting oxidation reaction that results in the production of $H_2O_2$. The data are most consistent with a reaction mechanism that proceeds via cyclization-oxidation-dehydration during in vitro maturation under aerobic conditions. The ejection of water from the heterocycle that is formed from main chain protein atoms appears to depend on the degree of $\pi$-overlap of the five-membered ring with the side chain adduct.

**Keywords:** Green fluorescent protein, chromophore biogenesis, hydrogen peroxide evolution, intrinsic cofactors, tyrosine oxidation

## 1. INTRODUCTION

Most researchers are familiar with green fluorescent protein (GFP) as a fusion tag to report on cellular events (*1*). Due to its intrinsically bright color, GFP is easy to visualize and can be used to precisely localize sub-cellular events. The family of GFP-like proteins has a profound impact on the versatility of techniques available to cell biologists studying diseases ranging from cancer to developmental disabilities to genetic defects. Highly sensitive fluorescence microscopes, used in conjunction with a large variety of gene-based fluorescent probes, provide the researcher with powerful tools to resolve cellular events (*2-4*). Close to two hundred new publications on GFP-related research appear in the PubMed data base each month, and many biomedical applications for GFP as a non-invasive visual reporter can be enumerated. For example, embryonic stem cells derived from GFP-transgenic mice have been implanted into normal mice and mouse models for disease states. With this technique, the fate of implanted donor cells can be monitored visually (*5*). The development of therapies for a large number of genetic and neurodegenerative disorders can be facilitated by monitoring disease progression non-invasively in mouse models (*6*).

In this work, we report on recent advances in our research on the chemistry of protein post-translational modifications, especially protein self-processing reactions, reactions that lend the protein unusual biochemical or biophysical properties. As it turns out, some aspects of the GFP self-modification process are reminiscent of other kinds of protein post-translational modifications, and some aspects are quite unique to the family of GFP-like proteins. An important class of protein post-translational modifications proceeds via oxidative tyrosine modifications, in which molecular oxygen serves as the final electron acceptor. A good example is the biosynthesis of quinone-type cofactors. These are redox cofactors derived from the modification of tyrosine residues, such as topaquinone (TPQ) and pyrroloquinoline quinone (PQQ) (*7*). TPQ is found in the copper amine oxidases, and is a prosthetic group covalently linked to the protein's polypeptide chain

* Corresponding Author. Email RWachter@asu.edu, phone 480-965-8188, fax 480-965-2747

Genetically Engineered Probes for Biomedical Applications, edited by Alexander P. Savitsky, Rebekka Wachter,
Proc. of SPIE Vol. 6098, 609803, (2006) · 1605-7422/06/$15 · doi: 10.1117/12.648542

(*8*). Completion of the self-modification reaction that takes about 20 min, and involves the oxidation of a specific tyrosine residue. The reaction is autocatalytic and requires a redox-active metal ion. In PQQ biogenesis, however, no redox-active metals or cofactors involved. Biosynthesis involves expression of six genes, and the cofactor is constructed

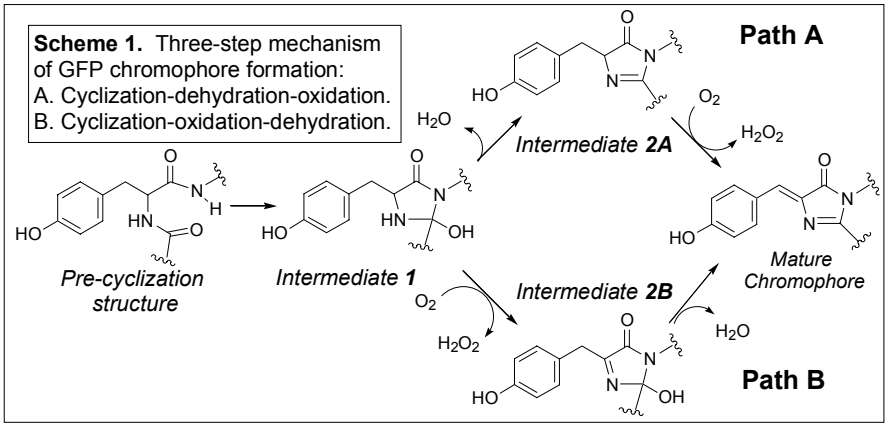


from a tyrosine and a glutamate residue of a 23 residue precursor peptide (*9*). In GFP, a bright green-fluorescent chromophore is generated spontaneously from internal protein residues. The modification also involves a tyrosine oxidation reaction. However, oxidation does not occur at aromatic ring positions, but instead occurs along the tyrosine Cα-Cβ bond (*1*). In addition, no metal ions are involved to mediate the transfer of electrons to molecular oxygen. Several interesting questions arise: What role does the aromaticity play in the oxidative process? Is the tryrosine ring involved in oxygen activation? How is molecular oxygen activated without the aid of any redox active metal ions? Which protein-derived groups trigger the protein's sensitivity to molecular oxygen?

To consider these questions more carefully, it is important to note that a number of tyrosine modifications also involve internal protein cross-linking reactions. Cross-linking reactions tend to be auto-catalytic events, in that the protein fold catalyzes its own modification. Examples are oxidative reactions that connect side-chain atoms, such as the thioether bridge between a tyrosine and cysteine residue in galactose oxidase (*10*), or the aromatic-aromatic cross-link in the catalase-peroxidase (*11*). Alternatively, main-chain condensation reactions that are nucleophilic addition-elimination reactions have been described in a few enzymes such as the ammonia lyases (*12*) and a tyrosine amino mutase (*13*), as well as in the family of GFP-like proteins (*14*). These cross-linking reactions are ways to generate built-in redox cofactors or electrophilic cofactors important in enzyme catalysis, or to generate a light-activated prosthetic group important in protein coloration. We are currently using GFP as a model system to understand peptide backbone cyclo-addition reactions, and to understand the mechanism of oxygen reduction by protein-derived groups.

The GFP fold consists of an eleven-stranded beta barrel with a helix threaded through the center of the barrel (*15*). This helix carries three residues that are modified to form a chromophore, Ser65, Tyr66, and Gly67. We would like to know what drives the modification process in GFP. Why does this chemistry occur spontaneously in GFPs but not more generally in all kinds of proteins? In all GFP-like proteins, the first step after protein folding is a backbone condensation reaction that leads to a cyclic intermediate. This intermediate can be trapped by two different mechanisms. According to Path A (Scheme 1), the high-energy cyclic state is trapped via dehydration. Water is ejected from the heterocycle, and the oxidation process proceeds from intermediate 2A. Slow oxidation yields the mature chromophore and a reduced oxygen species such as hydrogen peroxide (*16*). According to path B, the sequence of oxidation and dehydration is essentially reversed (Scheme 1). The high-energy cyclic intermediate is trapped via slow oxidation of the five-membered ring. Here, dehydration of the ring is the last step and leads directly to the mature chromophore.

## 2. MATERIALS AND METHODS

### 2.1 Site-directed mutagenesis and protein preparation

Amino acid replacements were introduced into EGFP (GFP-F64L/S65T) using the PCR-based QuikChange Site-directed Mutagenesis Kit (Stratagene). Expression of N-terminally 6His-tagged protein and purification by Ni-NTA affinity

chromatography were carried out as described in references (*17, 18*). To prepare inclusion bodies, the culture growth temperature was equilibrated to 42º (*19*), and inclusion bodies were solubilized and purified in the presence of 8M urea (*18*).

**2.2 Chromophore formation kinetics of R96M and E222Q**
Procedures were carried out as described in reference (*18*). Briefly, the rate of chromophore formation was monitored as a function of pH by determining the increase in visible absorbance with time. The data were computer-fitted to a unimolecular reaction rate equation. Pseudo-first order rate constants were computer-fitted to a rate expression for a base-catalyzed reaction with a rapid preliminary equilibrium.

**2.3 Maturation kinetics of EGFP prepared from inclusion bodies**.
Procedures were carried out as described in reference (*18*). Briefly, inclusion bodies of EGFP were prepared and purified in 8 M urea, and protein folding was induced by rapid dilution. The change in absorbance at 489 nm (native-state chromophore anion) was fitted to a unimolecular rate equation.

**2.4 Trypsinolysis, peptide purification and MALDI mass spectrometry**
Procedures were carried out as described in references (*18, 20*). Briefly, trypsin digests were carried out at a weight ratio of 1:2 trypsin:GFP, and tryptic peptides were separated by reverse-phase HPLC on a C18 analytical column. Eluting peptide fractions were collected, lyophilized, and analyzed by MALDI.

**2.5 Preparation of yellow EGFP-Y66L**
Procedures were carried out as described in reference (*21*). Colorless Y66L was converted to a UV/Vis absorbing form with yellow appearance by incubation in the presence of 2.0 M sodium formate. The UV/Vis absorbance was monitored for three weeks at pH 6.5 and pH 8.0. Incubations were also carried out under anaerobic conditions, followed by switching to an aerobic atmosphere.

**2.6 Crystallization and structure determination of EGFP-Y66L**
Procedures were carried out as described in references (*17, 21*). EGFP-Y66L was expressed in soluble form and crystallized via the hanging-drop vapor diffusion method with polyethylene glycol as precipitant. In-house X-ray diffraction data were collected to 1.5 Å and 2.0 Å, processed in spacegroup $P2_12_12_1$, and the structures were solved by molecular replacement using the structure of GFP-S65T (*15*) as a search model.

**2.7 GFP maturation monitored via hydrogen peroxide evolution and chromophore fluorescence**
Procedures were carried out as described in reference (*20*). The GFP-trix variant (GFP-F64L/S65T/F99S/M153T/V163A/A206K) was prepared by site-directed mutagenesis using EGFP as the parent clone. Inclusion bodies of GFP-trix were prepared as described (*17*), and maturation was induced using the procedures described in reference (*18*). Hydrogen peroxide assays were carried out using the Amplex Red® Hydrogen Peroxide Assay Kit (Molecular Probes, Inc.) (*22*), monitoring the formation of resorufin by its red fluorescence. GFP chromophore formation was monitored via green fluorescence. Global curve-fitting procedures were carried out using the program DynaFit™(*23*), and the rates of resorufin and GFP chromophore production were fitted to a sequential three-step mechanism for GFP maturation.

**2.8 GFP maturation monitored by HPLC and MALDI**
Procedures were carried out as described in reference (*20*). For each GFP maturation time point, the reaction mix was injected into a reverse-phase C4 HPLC column and the protein was eluted using a linear water-acetonitrile gradient. Protein fractions were collected, lyophilized and their masses determined by MALDI.

## 3. RESULTS AND DISCUSSION

**3.1 Catalysis of cross-linking reaction by the protein fold**
Several X-ray structures have demonstrated that backbone cyclization is a prerequisite for the rate-limiting protein oxidation step (*24*). Though there appears to be a large degree of structural pre-organization to bring the reacting main-chain atoms into close proximity (*25*), proper conformational alignment in itself does not account for the rate of self-catalysis. Two charged residues directly adjacent to the chromophore are highly conserved, Arg96 and Glu222 (*26*).

These two residues are found in buried positions, and Arg96 is directly hydrogen-bonded to the chromophore (*15*). The obvious interpretation is that these residues carry out important catalytic functions in generating the chromophore (*1*).

To examine the catalytic roles of Arg96 and Glu222 in more detail, we prepared a series of mutants (*27*), and measured their rate of chromophore formation as a function of pH. We prepared these mutations in EGFP (Enhanced GFP) background (*28*). In intact GFP, we do not observe any pH dependence of in vitro maturation, which proceeds with a time constant of about 1 hour between pH 7 and 10 (*18*). Two mutants gave particularly interesting kinetic results: In R96M, the positive charge has been removed, and in E222Q, the negative charge has been removed. Both variants exhibited significant pH dependence. At pH 8.0, EGFP-R96M maturation proceeded extremely slowly with a time constant of 6.5 months, whereas E222Q maturation proceeded over many hours, with a time constant of 7.4 hours. In both cases, significant rate-acceleration was observed at elevated pH, and the data could be fit to a base-catalyzed reaction with a rapid preliminary equilibrium. Apparently, the reaction rate depends on a titratable protein group that is catalytically active in the deprotonated form only (*18*). From the curve fits, we have extracted pKa values of 6.5 in R96M and 9.2 in E222Q. We have tentatively assigned a pKa of 6.5 to the Glu222 carboxylate in R96M and a pKa of 9.2 to the glycine 67 amide nitrogen in E222Q.

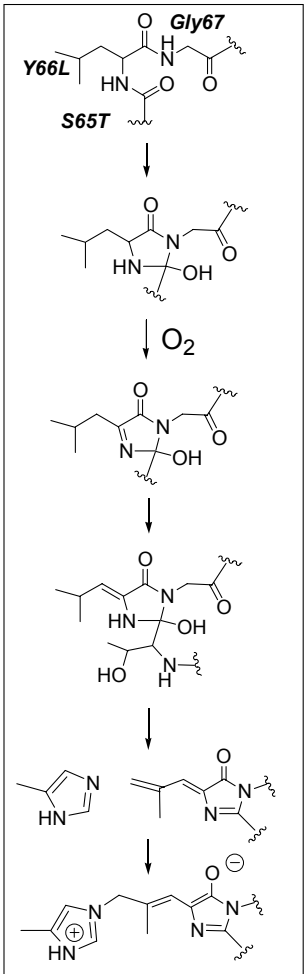


**Scheme 2.** Oxidative self-modification process in EGFP-Y66L, and cross-link formation with His148.

What sort of mechanistic model can account for the observed rates and pKa values? Arg96 clearly functions as an electrophile, and Glu222 appears to function as a general base, catalyzing essential proton transfer reactions. The Arg96 hydrogen bond to the amide oxygen leads to an acidification of the amide nitrogen, as well as the alpha-carbon, and the apparent pKa is estimated to be about 9. A drop of the peptide bond pKa value from about 15 to 9 is not unreasonable based on small-molecule model studies on acetamide (*29*). A plausible mechanistic model would suggest that Glu222 aids in generating the Gly67 amide anion by accepting a proton, in preparation for nucleophilic attack of the amide anion nitrogen onto the carbonyl carbon of Ser65. After ring closure, Glu222 may also be responsible for removal of the α-proton of residue 66 to generate the α-enolate. Enolization appears to be essential in trapping of the cyclized intermediate, be via dehydration or oxidation. The cyclization reaction can also be written in a different order, where proton removal at the Tyr66 α-carbon is the first step, i.e. the cyclo-addition reaction is initiated by enolization. We are currently devising ways to distinguish between these possibilities.

In the E222Q variant, there appears to be a change in mechanism from general to specific base catalysis. When the glutamic acid is removed, tremendous rate acceleration is observed at high pH. The interpretation is that at high pH, the amide bond is in equilibrium with the amide anion, with a pKa of about 9. We have proposed that specific base catalysis is responsible for the very rapid rate of chromophore formation in E222Q at high pH (*18*). At pH 9.5, the maturation rate of E222Q is three to four times faster than in intact GFPs such as EGFP, suggesting that base catalysis may be important in the rate-determining steps of chromophore biosynthesis in intact variants as well.

### 3.2 Role of the aromatic group of Tyr66

Some years ago, in vivo experiments demonstrated that the rate-limiting process in GFP maturation depends on the availability of molecular oxygen. It is as yet unknown whether GFP oxidation is slow because of weak $O_2$ binding, slow slow electron transfer to molecular oxygen to generate the superoxide anion radical, or slow proton transfer reactions that are necessary for $O_2$ reduction. However, dioxygen is activated by the GFP fold in some way the absence of metal ions. Is the oxidation step dependent on the aromaticity of Tyr66, in analogy to other oxidative tyrosine modifications? Does the Tyr66 phenolic group play a role in the oxidation reaction?

Substitution of Tyr66 with a leucine eliminates the visible absorbance band, and the Y66L variant is colorless (*17*). We solved the X-ray structure of this variant, and found that the backbone has indeed condensed to form a 5-membered ring.

Clearly, the tyrosine is not essential for the cyclization reaction. In addition, we found that the tetrahedral intermediate was trapped in colorless Y66L. The hydroxyl leaving group remained attached to the heterocycle in the presence of an aliphatic side chain derived from residue 66. To our surprise, the electron density was consistent with a trigonal planar geometry around the α-carbon of residue 66. The most plausible explanation is that the ring has been oxidized to the cyclic imine form (Scheme 2), and using MALDI mass spectrometry, we have verified a mass loss of 2 Daltons in colorless Y66L (*18*). We conclude that the aromaticity of Tyr66 is not essential for the oxidation either, and that the hydration adduct is stable in the oxidized form of the heterocycle.

**3.3 The mechanism of GFP chromophore formation is mimicked in Y66L**

We found that under some conditions, a yellow chromophore absorbing around 400 nm is generated in the Y66L variant. This process appeared to be facilitated by aerobic conditions in the presence of a general base such as 2 M formate. We also found that the yellow species is generated from an intermediate that absorbs at 338 nm, and that formation of the 338-nm species is independent of oxygen. The X-ray structure of yellow Y66L indicated nearly complete elimination of water from the heterocycle (*21*). The electron density of the leucine side chain appeared to be in a near-planar conformation, most consistent with π-orbital conjugation of the side chain atoms with the heterocycle. At low pH, we made the astounding discovery of a covalent cross-link between the Leu-derived side chain and a near-by His imidazole ring. Again, we observed co-planarity of the Leu-drived side chain with the heterocycle. In addition, the electron density was consistent with complete ring dehydration.

The most plausible interpretation is that the mechanism of chromophore formation is mimicked in Y66L, though with altered reaction energetics (Scheme 2). Colorless Y66L (cyclized and oxidized) appears to slowly dehydrate to generate the analog of the mature GFP chromophore, absorbing at 338 nm in analogy to the MIO cofactor in the ammonia lyases (*30*). Dehydration appears to be facilitated by a general base, possibly to remove the residue 66 β-proton. The Y66L analog of the GFP chromophore is apparently sensitive to activated oxygen species, and slow oxidation eventually yields a doubly desaturated side chain adduct that is responsible for the yellow color. Clearly, an analog of the mature GFP chromophore must be the precursor to yellow Y66L. The cross link observed in one of the X-ray structures (*21*) is likely generated by a Michael-type conjugate addition reaction, in which the His148 imidazole initiates nucleophilic addition to the highly electrophilic diene derived from the Leu66 side chain (Scheme 2). This chemistry suggests that the electrophilic diene could be used as a covalent attachment site to attach functional groups to the protein scaffold.

The mechanistic implications of the Y66L work can be summarized as follows. In Y66L, the 338 nm species is chemically similar to the histidine ammonia lyase cofactor MIO, and absorbs in the same region of the spectrum (*30*). The 338-nm species is the Y66L analog of the GFP chromophore, and is generated via a cyclization-oxidation-dehydration mechanism. This reaction is analogous to Path B in GFP chromophore formation (Scheme 1). Though these data do not provide information as to whether the GFP maturation mechanism proceeds in the same order, it can be concluded that GFP chromophore biogenesis is not driven by the aromatic character of Tyr66. The crystallographic structures obtained for various Y66L forms provide evidence that a hydration-dehydration equilibrium may exist in the interior of the protein. In colorless Y66L bearing an aliphatic Leu-derived side chain, we observe the hydration adduct only (0% of the heterocycle is dehydrated). In the yellow forms, the heterocycle is primarily dehydrated, and the side chain is mostly desaturated. In the cross-linked yellow form, the ring is 100% dehydrated, and the side chain is entirely conjugated, with no crystallographic evidence of mixed species. We conclude that the ejection of water from the 5-membered ring is favored upon extensive π-conjugation with the side chain adduct. Therefore, the aromatic ring of the tyrosine residue in intact GFP may play a role in favoring dehydration to complete the process of chromophore formation.

**3.4 Reaction progress in intact GFPs**

A large amount of information has been gleaned from the mutant studies regarding the more general features of the GFP self-processing reaction. However, to understand what factors limit the rate of intact GFP maturation, it is imperative to dissect the oxidation reaction into individual microscopic steps. To this end, we have defined the reaction progress in intact GFP in greater detail. To study the reaction progress, immature protein isolated from inclusion bodies was used as starting material (*19*), since this protein does not contain a chromophore due to misfolding in the cell. Protein folding was initiated by rapid dilution from urea, and a variety of techniques were employed to monitor the reaction progress, such as hydrogen peroxide evolution, acquisition of green fluorescence, HPLC and MALDI (*20*). Hydrogen peroxide is the putative co-product generated by oxygen reduction during GFP maturation. To detect peroxide, we have employed a

fluorogenic enzyme-linked assay based on Amplex Red™ (*22*). In the presence of peroxide and horseradish peroxidase, the colorless reagent is oxidized to resorufin, which is bright red fluorescent. Though resorufin is a hydrogen peroxide indicator, the response is not instantaneous. Under our assay conditions, the time constant for development of red fluorescence is 9 min, using a uni-molecular reaction rate approximation.

Using this assay, peroxide production was monitored continuously during GFP maturation from inclusion bodies by the development of resorufin fluorescence. In addition, GFP chromophore formation was monitored continuously by the development of green fluorescence (*20*). Since the development of red fluorescence (resorufin) from hydrogen peroxide proceeds with a time constant of 9 min, whereas chromophore fluorescence is detected in real time, the data indicate that peroxide must be generated prior to the GFP chromophore. Therefore, the oxidation step must occur prior to the last step in GFP maturation. All experimental progress curves were fitted to a three-step mechanism for chromophore formation, using global curve fitting procedures using the program DynaFit™(*23*). The mechanism most consistent with experiment is one in which the oxidation step is the second step. From the curve fit, the estimated time constants were 1.5 min for folding and cyclization, 34 min for oxidation, and 11 min for the final step that completes the process, proposed to be dehydration. The curve-fitting procedure allows for calculation of progress curves for each species involved. Therefore, total hydrogen peroxide produced by the protein can be calculated by the numerical addition of the resorufin and free hydrogen peroxide concentrations. Clearly, hydrogen peroxide evolution precedes the final step in chromophore formation, and oxidation is the major rate-limiting event, though the third and final step also contributes to rate retardation (*20*). The results of the global curve fitting procedures are most consistent with Path B (Scheme 1), where oxidation proceeds from an early intermediate, intermediate 1, to yield the oxidized intermediate 2B. According to this interpretation, intermediate 2B is the species trapped in the colorless Y66L variant, where the X-ray structure is consistent with an $sp^2$-hybridized α-carbon in the hydration adduct form of the ring (*17*). The mechanism in Path B also supports the notion that ring dehydration becomes energetically more favorable once the Tyr66 α–β bond is desaturated, thus allowing for more extensive conjugation. The maturation conditions used to determine rate constants involved a well-aerated aqueous solution with dissolved $O_2$ concentrations estimated in the low micromolar range. However, in the cellular environment, oxygen concentrations may be lower and be a function of the particular cellular compartment. Therefore, it is possible that oxygen concentrations have some effect on whether Path A or Path B is more populated (Scheme 1).

**3.5 Accumulation of reaction intermediates**

To identify intermediate species on the reaction pathway, we developed an HPLC assay in which we were able to separate precursor species from intermediates. In this assay, the precursor elutes later than the intermediate species, and the intermediates co-elute with the mature species (*20*). Chromophore formation can be monitored by 380nm absorbance. Control experiments indicate that the late-eluting peak consists of pre-cyclization species, and the early-eluting peak consists of post-cyclization species. Precursor and the major intermediate species appear to be in equilibrium with each other under acidic HPLC conditions, which are denaturing conditions. Hence, information regarding the position of this equilibrium in the folded protein cannot be determined from these data. However, HPLC peaks collected at designated time points were digested with trypsin, the peptides were isolated, and their masses determined by MALDI (*18*). Masses of tryptic peptides that bear the chromophore-forming residues TYG indicate that in the post-cyclization peak, a mass loss of 2 Da is consistently observed, in addition to the unmodified peptide and the mature protein species with a mass loss of 20 Da. In the pre-cyclization species, only unmodified peptides were observed, as expected. These results support the interpretation that an oxidized protein intermediate accumulates during the reaction, which has lost two hydrogen atoms, in further support of path B for GFP maturation in a well-aerated test tube.

**3.6 Proposed mechanism of oxidation via a hydroperoxy intermediate**

To guide our thinking, we have proposed a mechanism in which the α-enolate generated by deprotonation of the Tyr66 α-carbon is the oxygen-sensitive species. Formation of the α-enolate may be facilitated by Arg96 and Glu222, and reaction with molecular oxygen may generate a peroxy adduct to the five-membered ring(*17*). Concomitant with various proton transfer reactions, release of hydrogen peroxide is proposed to yield the cyclic imine, intermediate 2B (Scheme 1). Hydroperoxy intermediates have been proposed in several enzyme systems that utilize molecular oxygen in conjunction with organic cofactors, such as flavins and pterins (*31*). In these enzymes, the first electron transfer step to molecular oxygen limits the rate of cofactor re-oxidation, and proton transfer is decoupled from electron transfer. As

compared to enzyme turnover, GFP chromophore biogenesis is quite slow, one-half to one hour. Therefore, it is conceivable that proton transfer plays a more significant role in the slow GFP oxidation reaction.

## ACKNOWLEDGMENTS

This work was supported by National Science Foundation (NSF), Grant MCB-0213091 (to R.M.W.). NSF Grant CHE-0131222 provided funds to purchase the mass spectrometer.

## REFERENCES

1. Tsien, R. Y. The Green Fluorescent Protein. (1998) *Ann. Rev. Biochem. 67*, 509-544.
2. Lippincott-Schwartz, J., and Patterson, G. H. Development and use of fluorescent protein markers in living cells. (2003) *Science 300*, 87-91.
3. Hanson, G. T., Aggeler, R., Oglesbee, D., Cannon, M., Capaldi, R. A., Tsien, R. Y., and Remington, S. J. Investigating mitochondrial redox potential with redox-sensitive green fluorescent protein indicators. (2004) *J. Biol. Chem. 279*, 13044-13053.
4. Dooley, C. M., Dore, T. M., Hanson, G. T., Jackson, W. C., Remington, S. J., and Tsien, R. Y. Imaging dynamic redox changes in mammalian cells with green fluorescent protein indicators. (2004) *J. Biol. Chem. 279*, 22284-22293.
5. Meyer, J. S., Katz, M. L., and Kirk, M. D. Stem cells for retinal degenerative disorders. (2005) *Ann. NY Acad. Sci. 1049*, 135-145.
6. Hadjantonakis, A. K., and Nagy, A. The color of mice: in the light of GFP-variant reporters. (2001) *Histochem. Cell Biol. 115*, 49-58.
7. Okeley, N. M., and van der Donk, W. A. Novel cofactors via post-translational modifications of enzyme active sites. (2000) *Chem. Biol. 7*, R159-171.
8. Schwartz, B., Dove, J. E., and Klinman, J. P. Kinetic analysis of oxygen utilization during cofactor biogenesis in a copper-containing amine oxidase from yeast. (2000) *Biochemistry 39*, 3699-3707.
9. Magnusson, O. T., Toyama, H., Saeki, M., Rojas, A., Reed, J. C., Liddington, R. C., Klinman, J. P., and Schwarzenbacher, R. Quinone biogenesis: Structure and mechanism of PQQC, the final catalyst in the production of pyrroloquinoline quinone. (2004) *Proc. Natl. Acad. Sci. USA 101*, 7913-7918.
10. Firbank, S., Rogers, M., Guerrero, R. H., Dooley, D. M., Halcrow, M. A., Phillips, S. E., Knowles, P. F., and McPherson, M. J. Cofactor processing in galactose oxidase. (2004) *Biochem. Soc. Symp. 71*, 15-25.
11. Ghiladi, R. A., Medzihradszky, K. F., and de Montellano, P. R. O. Role of the Met-Tyr-Trp Cross-link in Mycobacterium tuberculosis catalase-peroxidase (KatG) as revealed by KatG(M255I). (2005) *Biochemistry 44*, 15093-15105.
12. Schwede, T. F., Retey, J., and Schulz, G. E. Crystal structure of histidine ammonia-lyase revealing a novel polypeptide modification as the catalytic electrophile. (1999) *Biochemistry 38*, 5355-5361.
13. Christenson, S. D., Liu, W., Toney, M. D., and Shen, B. A novel 4-mehylideneimidazole-5-one-containing tyrosine aminomutase in enediyne antitumor antibiotic C-1027 biosynthesis. (2003) *J. Am. Chem. Soc. 125*, 6062-6063.
14. Verkhusha, V., and Lukyanov, K. A. The molecular properties and applications of Anthozoa fluorescent proteins and chromoproteins. (2004) *Nat. Biotechnol. 22*, 289-296.
15. Ormo, M., Cubitt, A. B., Kallio, K., Gross, L. A., Tsien, R. Y., and Remington, S. J. Crystal structure of the *Aequorea victoria* Green Fluorescent Protein. (1996) *Science 273*, 1392-1395.
16. Cubitt, A. B., Heim, R., Adams, S. R., Boyd, A. E., Gross, L. A., and Tsien, R. Y. Understanding, improving, and using Green Fluorescent Proteins. (1995) *Trends Biochem. Sci. 20*, 448-455.
17. Rosenow, M. A., Huffman, H. A., Phail, M. E., and Wachter, R. M. The crystal structure of the Y66L variant of green fluorescent protein supports a cyclization-oxidation-dehydration mechanism for chromophore maturation. (2004) *Biochemistry 43*, 4464-4472.
18. Sniegowski, J. A., Lappe, J. W., Patel, H. N., Huffman, H. A., and Wachter, R. M. Base catalysis of chromophore formation in Arg96 and Glu222 variants of green fluorescent protein. (2005) *J. Biol. Chem. 280*, 26248-26255.

19. Reid, B. G., and Flynn, G. C. Chromophore formation in green fluorescent protein. (1997) *Biochemistry 36*, 6786-6791.
20. Zhang, L., Patel, H. N., Lappe, J. W., and Wachter, R. M. Reaction progress of chromophore biogenesis in green fluorescent protein. (2006) *J. Am. Chem. Soc. (submitted)*.
21. Rosenow, M. A., Patel, H. N., and Wachter, R. M. Oxidative chemistry in the GFP active site leads to covalent cross-linking of a modified leucine side chain with a histidine imidazole: Implications for th mechanism of chromophore formation. (2005) *Biochemistry 44*, 8303-8311.
22. Zhou, M., Diwu, Z., Panchuk-Voloshina, N., and Haugland, R. P. A stable nonfluorescent derivative of resorufin for the fluorometric determination of trace hydrogen peroxide: Applications in detecting the activity of phagocyte NADPH oxidase and other oxidases. (1997) *Anal. Biochem. 253*, 162-168.
23. Kuzmic, P. Program DYNAFIT for the analysis of enzyme kinetic data: Application to HIV protease. (1996) *Anal. Biochem. 237*, 260-273.
24. Barondeau, D. P., Putnam, C. D., Kassmann, C. J., Tainer, J. A., and Getzoff, E. D. Mechanism and energetics of green fluorescent protein chromophore synthesis revealed by trapped intermediate structures. (2003) *Proc. Natl. Acad. Sci. USA 100*, 12111-12116.
25. Barondeau, D. P., Kassmann, C. J., Tainer, J. A., and Getzoff, E. D. Understanding GFP chromophore biosynthesis: Controlling Backbone cyclization and modifying post-translational chemistry. (2005) *Biochemistry 44*, 1960-1970.
26. Matz, M. V., Fradkov, A. F., Labas, Y. A., Savitsky, A. P., Zaraisky, A. G., Markelov, M. L., and Lukyanov, S. A. Fluorescent proteins from nonbioluminescent Anthozoa species. (1999) *Nature Biotechnol. 17*, 969-973.
27. Sniegowski, J. A., Phail, M. E., and Wachter, R. M. Maturation efficiency, trypsin sensitivity, and optical properties of Arg96, Glu222, and Gly67 variants of green fluorescent protein. (2005) *Biochem. Biophys. Res. Comm. 332*, 657-663.
28. Cormack, B. P., Valdivia, R. H., and Falkow, S. FACS-optimized mutants of the Green Fluorescent Protein (GFP). (1996) *Gene 173*, 33-38.
29. Martin, R. B., and Hutton, W. C. Predominant N-bound hydrogen exchange via O-protonated amide. (1973) *J. Am. Chem. Soc. 95*, 4752-4754.
30. Rother, D., Merkel, D., and Retey, J. Spectroscopic evidence for a 4-methylidene imidazol-5-one in histidine and phenylalanine ammonia-lyases. (2000) *Angew. Chem. Int. Ed. 39*, 2462-2464.
31. Klinman, J. P. Life as aerobes: are there simple rules for activation of dioxygen by enzymes? (2001) *J. Biol. Inorg. Chem. 6*, 1-13.